LANGMUIR Article
Cite This: Langmuir 2019, 35, 4238−4245
pubs.acs.org/Langmuir

Bulk Nanobubbles Fabricated by Repeated Compression of Microbubbles

Juan Jin, Zhenqiang Feng, Fang Yang,* and Ning Gu*

State Key Laboratory of Bioelectronics, Jiangsu Key Laboratory for Biomaterials and Devices, School of Biological Sciences and Medical Engineering, Southeast University, Sipailou 2, Nanjing, Jiangsu 210009, P. R. China

Supporting Information

ABSTRACT: Nanobubbles (NBs), given its extraordinary properties, have drawn keen attention in the field of nanotechnology worldwide. However, compared to that of surface NBs, generation of stable bulk NBs remains an arduous task with the prevailing method. In this study, we developed a pressure-driven method to prepare bulk NBs by repeatedly compressing sulfur hexafluoride (SF_6) gas into water. The results show that NBs with a mean diameter of 240 ± 9 nm and a polydispersity index of 0.25 were successfully prepared. The generated NBs had a high negative zeta potential (−40 ± 2 mV) with stability of more than 48 h. Under the condition of 600 times repeated compression, the NB concentration could reach about 1.92×10^{10} bubbles/mL. Furthermore, we examine the possible formation mechanism involved in NB generation by virtue of optical microscopy and attenuated total reflectance Fourier transform infrared (ATR−FTIR) spectroscopy. The microscopic results showed that microbubbles about 10−50 μm formed first and then decreased to be nanoscale-sized. A stronger hydrogen bond was detected by ATR−FTIR spectroscopy during the shrinking of microbubbles into NBs. It is speculated that the disappearance of microbubbles contributes to the formation of NBs, and the strong hydrogen bond at the gas−water interface prompts the stability of NBs. Therefore, repeated compression of the gas in aqueous solution could be a new method to prepare stable nanosized bubbles for wide applications in the future.

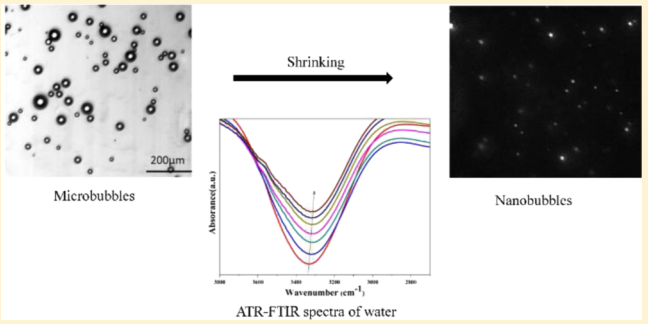

ATR-FTIR spectra of water

INTRODUCTION

Recently, free nanobubbles (NBs) have drawn great attention and been studied for decades because of their unique physicochemical properties. NBs can be divided into two categories: surface NBs and bulk NBs. The bulk NBs are gaseous domains surrounded by water, with a radius of typically tens to hundreds of nanometers.[1] The bulk NBs have many excellent properties including small size, large surface area, rapid attachment to hydrophobic surfaces, high stability, and so forth.[2] These particularities make bulk NBs have great potential in the applications of many areas such as water treatment[3] and cleaning,[4] acceleration of metabolism in vegetable/animal species,[5] biomedical diagnosis,[6] and treatment.[7,8]

Many experimental observations have shown that NBs (both surface and bulk NBs) are quite stable.[9−11] Evidences such as atomic force microscopy,[12,13] cryo-scanning electron microscopy,[14] transmission electron microscopy (TEM),[15] and total internal reflection fluorescence microscopy[16,17] have been reported to demonstrate the existence of NBs. In the case of surface NBs, different mechanisms including contact line pinning,[18−20] local supersaturation of the dissolved gas,[21] permeability of the gas−water interface,[22] and so on have been proposed to explain their unexpected long lifetime. However, there is a relatively fewer investigation on the long lifetime of bulk NBs. Theoretically, according to the Laplace and Young equation, $\Delta P = 2\gamma/r$, when the radius of a bubble decreases to nanoscale, the pressure inside the NB is too high to last more than a second. Thus, it seems that it is not possible for the NBs to remain in the solution. The sparked debate whether NBs are stable enough to be observed lasts for about a decade. Several models for the stability of a bulk NB have been proposed as reviewed by Yasui et al.[23] The dynamic equilibrium model is believed to be the most promising one, as directly evidenced by the TEM images. However, until now, there is no widely accepted explanation for their existence and stability.

In recent years, various techniques such as sonication,[24,25] electrolysis,[26−28] gas mixing, and supersaturation[29] for bulk NB fabrication have been proposed. However, most of the reported methods produce mixed micro- and nanoscale bubbles with multimodal size distribution. A further separation process is needed to obtain uniform NBs. Oh and Kim[10] fabricated uniform-sized NBs by mixing carbon dioxide (CO_2) gas with distilled water, but the concentration of NBs is relatively low. To prepare the concentrated and uniform bulk NBs, in this study, a novel and general approach to generate

Received: December 29, 2018
Revised: January 31, 2019
Published: February 28, 2019

DOI: 10.1021/acs.langmuir.8b04314
Langmuir 2019, 35, 4238−4245

stable bulk NBs was developed. The bulk NBs were generated by repeatedly compressing sulfur hexafluoride (SF_6) gas into water under high pressure and then returning to the standard atmosphere. The influence factors involved in NB generation and the stability of the generated NBs were investigated in detail. The formation process of NBs was monitored by optical microscopy and attenuated total reflectance Fourier transform infrared (ATR−FTIR) spectroscopy. The possible stabilizing mechanism of NBs was proposed which may provide a promising approach to fabricate shell-encapsulated NBs for future biomedical applications.

EXPERIMENTAL SECTION

Materials. Ultrapure water with a conductivity of 18.25 Ω/cm was prepared using a deionized (DI) water purification system. SF_6 with a purity of 99.99% was purchased from Anhui Qiangyuan Gas Co., Ltd. (Wuhu, China). Glass vials (3 mL) with open screw caps containing Teflon-covered silicon rubber septa and a 5 mL syringe fitted with a 22 G needle were used to produce NBs. All of them were repeatedly cleaned to eliminate nanosized impurities.

Generation of NBs in Water. DI water (2 mL) was added into a glass vial (3 mL) that was then capped with open screw caps containing Teflon-covered silicon rubber septa. The above air in the vial was replaced with SF_6 gas. A 5 mL syringe with a needle containing 3 mL SF_6 gas was connected to the vial. . The tip of the needle was kept 3 mm below the water surface. The septa and syringe were tested for leakage at the required pressure to ensure no detectable release of gas from the glass vial. Then, NBs were generated through a repeated change of pressure in the vial. As shown in Figure 1, the pressure can be changed by the up-and-down movements of the plunger, as calculated from the vapor phase volume in the vial using Boyle' s law.

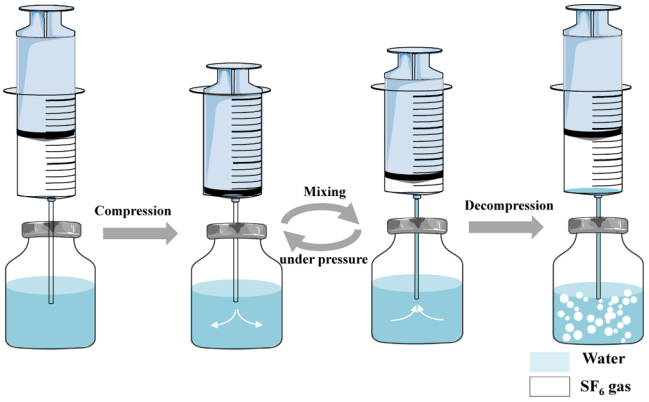

Figure 1. Schematic diagram of NB generation.

The typical process mainly included three steps: (1) compression: the gas was injected into water through a needle, and the maximum pressure was reached at this time; (2) mixing under pressure: repeated small volume (1 mL) changes by driving the fluids (gas and water) pass through the needle, resulting in the dissolution and mixing of gas in water above the atmospheric pressure; (3) decompression to atmosphere pressure: the local supersaturated gas in water was nucleated to form bubbles. The up-and-down movements of the plunger was driven by an electric motor, and the whole process was recorded as one compression cycle time. The operation was conducted at room temperature with different compression cycles.

Influence Factors on NB Generation and Stability. Factors such as the maximum pressure in the vial and the moving speed of the plunger that may affect the generation of bulk NBs were further investigated. The maximum pressure was regulated at 0.23, 0.30, 0.37, and 0.44 MPa by changing the gas volume, all of which were the gas oversaturation under pressure (SF_6 is a hydrophobic gas, and the solubility in water is 5.4 mL/L at 25 °C). The moving speed of the plunger was adjusted by the motor motion, and the effect of different speeds of 10, 20, and 30 mm/s on NB generation was investigated. Moreover, it would be necessary to verify the effect of pH on the generation and stability of NBs because the pH change may directly affect the adsorption of ions at the bubble interface. Thus, water with the preadjusting pH value from 1 to 12 was prepared by dropwise addition of HCl (4 M) or NaOH (4 M) to the distilled water at room temperature, respectively, which was monitored by a pH meter (FiveEasy, Mettler Toledo, Switzerland).

Size, Zeta Potential, and Concentration Measurements of NBs. The size distribution and zeta potential of NBs were analyzed by a Zeta-sizer (Nano ZS90, Malvern Instrument, United Kingdom). The refractive index of the material was set to 1.0 corresponding to air. All samples were measured without dilution. The visualization and concentration measurements of the generated NBs in solution were performed via a nanoparticle tracking analysis (NTA) instrument (NanoSight LM10 & NTA 2.0 Analytical Software, Malvern Instrument, United Kingdom). The NTA technique can monitor the motion of individual nanoparticles and provide the size and concentration of the samples because of its particle-by-particle measurement.[10,30] The obtained values of the mean size, zeta potential, and number of NBs are the arithmetically calculated values for a triplicate experiment.

To quantitatively detect the change of freshly generated microsized bubbles, a Multisizer (Multi 4e, Beckman, USA) was also used to measure the size distribution and concentration of the microbubbles. The bubble solution was measured at different times (0, 5, and 30 min) after preparation . The size detection range is from 1.34 to 30 μm. A 200 μL of bubble dispersion was added in 100 mL of electrolysis solution for the measurements.

Real-Time Monitoring of Microbubbles by Optical Microscopy. Optical microphotographs of bulk bubbles were captured by a real-time live cell optical imaging system (IX71, Olympus Co., Ltd., Japan). The freshly prepared NB dispersion was transferred immediately to a glass slide and monitored in real time at room temperature. The optical images of the microbubbles were observed and recorded over time. Video images were captured as digital images at 5 s intervals.

Detection of Water Molecules by ATR−FTIR. To investigate the structural changes of water in the presence of NBs, infrared (IR) broad bands for the O−H stretching vibration of the water molecule were detected by an attenuated total reflection spectrometer (IRAffinity-1, Shimadzu, Japan) with a horizontal ATR plate containing ZnSe crystal. When the bubble dispersion was prepared, the fresh sample was immediately added to the ATR plate and detected by ATR−FTIR at different times (0, 5, 10, 15, 20, 25, and 30 min). The infrared spectra were recorded with a resolution of 0.5 cm^{-1}, and a total of 20 scans were measured in the range of 450−4000 cm^{-1}. The analysis was performed isothermally at 298 K.

RESULTS

Generation of NBs in Water. An aqueous NB dispersion was fabricated by continued and repeated compression and mixing of SF_6 gas into water and decompression to atmospheric pressure. To examine the presence of nanosized impurities in DI water, dynamic light scattering (DLS) was performed, and no impurities were found (data not shown). After NB generation, Tyndall phenomenon was observed when a laser beam irradiated the aqueous NB solutions, whereas there was no light path in the DI water (Figure 2a). The observed Tyndall phenomenon suggests that stable nanosized particles were formed in water. It is very important to verify that the generated nanoparticles are actual gas-filled NBs. Alheshibri and Craig reported the methods to distinguish gas-filled NBs from nanoparticles by the evaluation of the compressibility and density of nanoparticles.[31,32] Here, we further studied the effect of freezing and thawing on NB

DOI: 10.1021/acs.langmuir.8b04314
Langmuir 2019, 35, 4238−4245

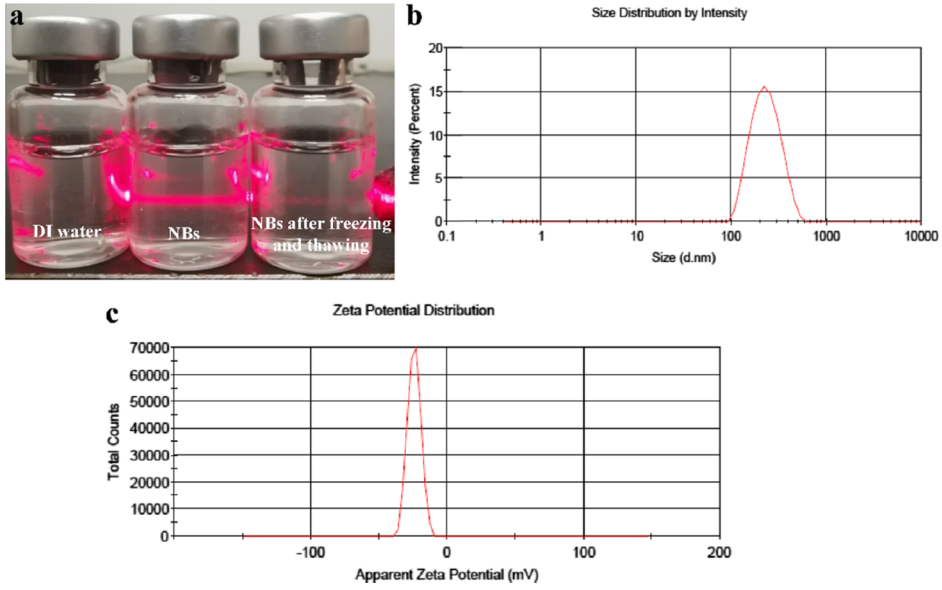

Figure 2. Characterization of the generated NBs. (a) Tyndall phenomenon of NB dispersion before and after freezing and thawing. (b) Size distribution of NBs. (c) Zeta potential distribution of NBs.

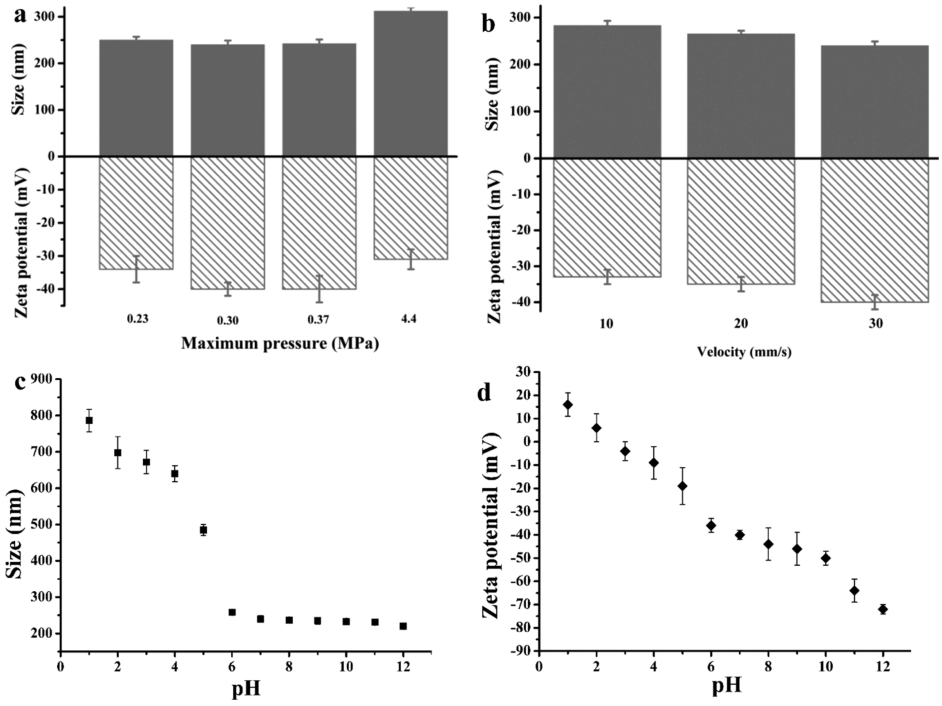

Figure 3. Effects of (a) maximum pressure in the vial, (b) moving speed of the plunger, and (c,d) preadjusted pH in water on the sizes and zeta potentials of NBs.

dispersion by keeping the samples at a temperature of −20 °C for 24 h and then leaving to thaw at room temperature. A very weak light path was observed in NB dispersion after freezing and thawing, as shown in Figure 2a. DLS measurements also showed a low detectable number of particles (the count rate changed from 280 to 300 to about 10 after freezing and thawing). Nirmalkar et al. verified that most of the contaminants of surfactants could be preserved against the effects of freezing and thawing.[30] Thus, the disappearance of the majority of "nanoparticles" during freezing and thawing implies the rupture of the gas-filled NBs. We also prepared infrared-active CO_2 NBs by this method, and the measured IR spectrum proved the existence of CO_2 gas in NBs (further details are described in the Supporting Information and Figure S1). These results further provide the evidence of gas-filled NBs.

Unlike pure DI water, NBs can be clearly detected by DLS, which is shown in Figure 2b. The NB size distribution showed a regular shape of a monomodal log-normal curve, and the measurements had good repeatability. The size distribution by intensity is from 100 to 600 nm, and the average size of NBs is 240 ± 9 nm. The polydispersity index (PDI) of the NBs is 0.25, indicating the uniform size of the produced bubbles. As a control, SF_6 gas was directly mixed with DI water in the same

DOI: 10.1021/acs.langmuir.8b04314
Langmuir 2019, 35, 4238−4245

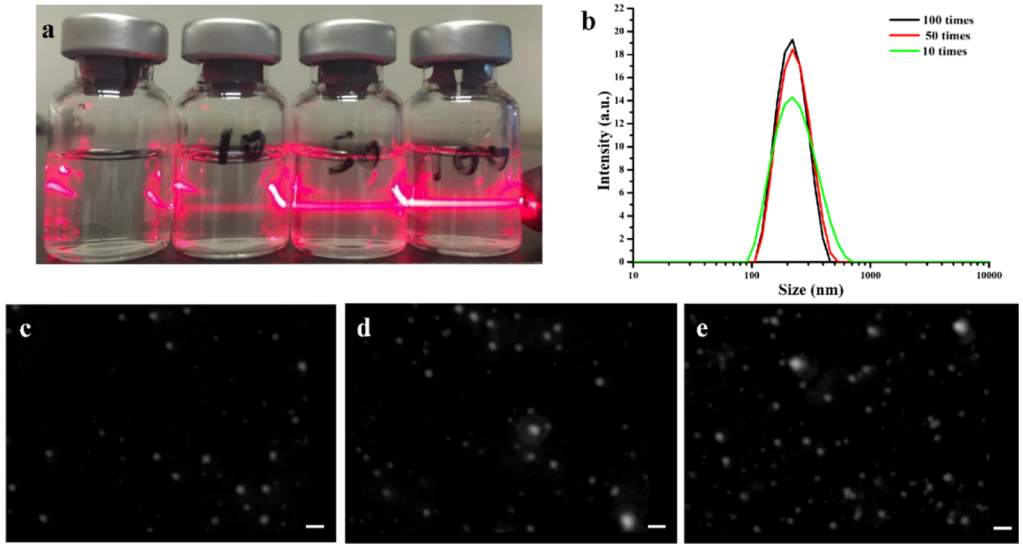

Figure 4. NB concentration controlled by compression times. (a) Tyndall phenomenon, (b) size distributions, and (c–e) NTA results of NB dispersion after 10, 50, and 100 compression times. Scale bar: 5 μm.

setup but just under the atmospheric pressure. It showed no particle detected.

An important property of NBs in solution is the negative zeta potential. The zeta potential of the solution was measured before and after NB generation. The average zeta potential value of water before compression is around zero. After the NB production, the average zeta potential value, as shown in Figure 2c, is −40 ± 2 mV with a typical single peak. It is reported that the surface of microbubbles is negatively charged and the zeta potential increases with the decrease of size because of the nano gas–water interface.[33] Therefore, the relatively high zeta potential of the solution further confirms the presence of NBs.

Influence Factors of NB Generation. The factors that may affect the generation of NBs were further investigated, and the results are displayed in Figure 3. Figure 3a shows the average sizes and zeta potentials of NBs generated under different maximum pressures. With the increase of the maximum pressure from 0.23 to 0.37 MPa, the size of the bubbles slightly decreases and the absolute value of the zeta potential gradually increases. When the pressure is high enough (0.44 MPa), the average size becomes larger (312 ± 8 nm) and the average zeta potential decreases to be −31 ± 3 mV. Also, the detectable number of particles by DLS is very low (the count rate showed small values about 30). These results indicate that only a few large bubbles are retained after generation under the maximum pressure of 0.44 MPa. The high pressure may lead to a high oversaturation to generate big bubbles that finally explode.

Figure 3b shows the effect of the moving speed of the plunger on the generation of NBs. The average size of NBs is 283 ± 10, 265 ± 7, and 240 ± 9 nm when the moving speed is 10, 20, and 30 mm/s, respectively. With the increase of the moving speed, the absolute value of the bubble zeta potential becomes larger and larger (−33 ± 2, −35 ± 2, and −40 ± 3 mV, respectively) accompanied by the decrease of size. High moving speed means a fast and complete mixing of gas and water, which results in the generation of smaller bubbles with high zeta potential.

The average size and zeta potential of the generated NBs in water with different pHs of 1–12 are shown in Figure 3c,d. The average size decreases as the water pH increases from 1 to 12. Monodispersed NBs can be generated at pH 6–12 (PDI 0.17–0.25, Table S1). However, the bubble suspension has a large PDI value, greater than 0.4, under strong acidic conditions (pH 1–5), indicating the formation of different-sized bubbles. As indicated in Figure 3d, the generated bubbles have negative zeta potential under a wide range of pH conditions (pH 3–12). The bubbles show positive zeta potential only in strong acid water below pH 3. The negative value increases with the increase of pH and reaches −72 mV at pH 12. High zeta potential means high colloidal stability, suggesting that NBs should be much more stable in alkaline solutions. These results are consistent with those obtained by other preparation methods in the literature.[30,33]

On the basis of the above results, the preparation parameters were chosen for further study as follows: maximum pressure of 0.3 MPa, moving speed of 30 mm/s, and water pH of 7 (DI water without the addition of ions).

NB Concentration Controlled by Compression times. The concentration of NBs can be regulated by compression times. The compression times used to generate NBs were 10, 50, and 100. Figure 4a shows the observed Tyndall phenomenon of the NB dispersion with different compression times. The light path appeared thicker and brighter in NB solution with the increase of compression times. These results indicate that more NBs were generated with the increase of compression times.

The sizes of NBs with different compression times were measured with DLS, as shown in Figure 4b. The intensity peak positions of NBs generated with different compression times maintained almost the same value (around 240 nm), but the intensities increased with the increase of compression times. The mean sizes of NBs generated with different compression times showed no significant differences.

Particle analysis using the NTA method was further performed to quantitatively investigate the concentrations of NBs in water. Figure 4c–e shows the particle analysis results of NBs with the same dilution factor prepared by different compression times. The measured NB concentrations with the compression times of 10, 50, and 100 were 7.62×10^8, 2.32×10^9, and 3.49×10^9 particles/mL, respectively (Table 1). The

DOI: 10.1021/acs.langmuir.8b04314
Langmuir 2019, 35, 4238–4245

Table 1. Size and Concentration of NBs Prepared with Different Compression Times

times	10	50	100	600
size (nm)	195 ± 72	183 ± 68	184 ± 71	175 ± 50
concentration (particles/mL)	7.62×10^8	2.32×10^9	3.49×10^9	1.92×10^{10}

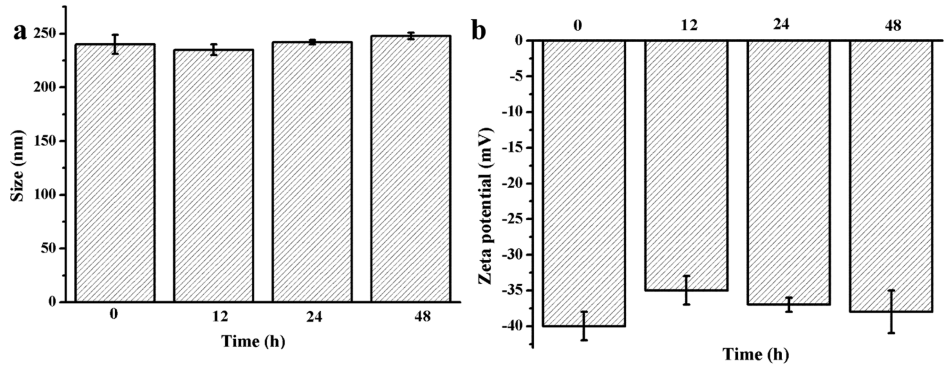

Figure 5. Stability of bulk NBs in water. (a) Average size and (b) average zeta potential of NBs over a period of 48 h.

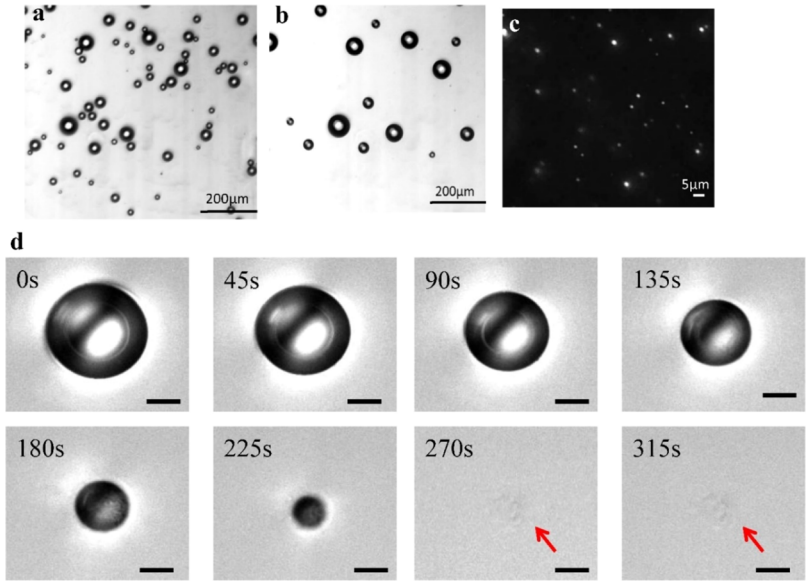

Figure 6. Optical image of bubbles in water (a) 0 and (b) 30 min after generation. (c) Laser-illuminated NBs in DI water. (d) Change process of one typical bubble over time. Scale bar: 10 μm.

results showed that the concentration of NBs is proportional to the compression times. It is worth pointing out that a higher concentration of 1.92×10^{10} can be obtained as shown in Table 1 when the compression times reached 600.

Stability of Bulk NBs in Water. To investigate the stability of the generated NBs, the evolution of the NB diameter and zeta potential over 48 h was studied, which is shown in Figure 5. The average diameters of NBs at times of 0, 12, 24, and 48 h were 240 ± 9, 235 ± 5, 242 ± 2, and 248 ± 3 nm, respectively, showing no significant differences in size during the storage period. These results reveal the relatively high stability of NBs in water, which is consistent with the other results that NBs can be stable for days or even months.[29] On the other hand, the zeta potential of the NBs in water was about −35 to −40 mV within 48 h. The sustaining high zeta potential also indicates the stability of NBs in water.

NB Formation Resulting from Microbubbles. We further investigate the possible formation mechanism of NBs. A milky solution consisting of microbubbles can be observed during the operation of the NB generator. The freshly prepared aqueous bubble dispersion was immediately dropped on the slide and observed by an optical microscope. The change in bubble morphology is shown in Figure 6a,b. Lots of bubbles of 10−50 μm size were observed just after the bubble fabrication at the very beginning. After about 30 min observation, most of the bubbles disappeared and only some big bubbles of about 50 μm were left.

To further investigate the change of bubbles, one typical bubble of the size of 30 μm was focused and observed. The optical microscopic images of the bubble at a time interval of 45 s were captured from the dynamic bubble change process (Video S1, Supporting Information). Figure 6d shows the typical shrinking process of the bubble. At the beginning of observation (0−135 s), the bubble shrinks slowly. With the decrease of the bubble size, the bubble shrinks faster during the time from 180 to 225 s. At the end of observation, the bubble disappears almost instantaneously (shown as red arrow). Because of the limitation of the resolution of the optical

DOI: 10.1021/acs.langmuir.8b04314
Langmuir 2019, 35, 4238−4245

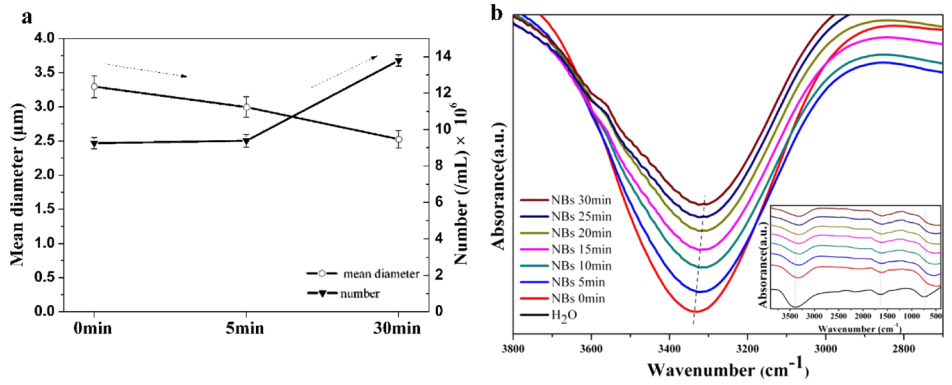

Figure 7. (a) Change of mean diameter and concentration of microbubbles after generation. (b) ATR−FTIR spectra for the O−H stretching mode in SF_6 bubbles dispersion at different times after generation. Inset is the overall spectra of water and bubble dispersions.

microscope, nanosized bubbles cannot be observed. However, after the disappearance of the microbubbles, the DLS and NTA results displayed the presence of stable NBs in water (Figure 6c). Bubbles are gas entities surrounded by water, and the interior gas is pressurized because of the increased surface tension of the gas−water interface. The bubble shrinks with the dissolution of the gas. According to the Laplace equation, $\Delta P = 2\gamma/r$, when the radius of the bubble decreases, the pressure inside the bubble increases and the bubble shrinks faster. We speculate that the formation of NBs is related to the shrinkage and disappearance of microbubbles.

ATR−FTIR Measurement of NBs from Microbubbles. The change of the freshly generated bubbles in micrometer scale was analyzed with a particle counter. Figure 7a shows the mean diameter and concentration of microbubbles at 0, 5, and 30 min after the preparation. A sharp peak near the lower limit can be recognized during the size measurement (Figure S2), and the peak grows up in accordance with the decrease and disappearance of big-sized microbubbles. The mean diameter of microbubbles decreases from 3.3 ± 0.2 to 2.5 ± 0.1 μm, and the concentration of microbubbles increases from (9.3 ± 0.3) to (13.8 ± 0.3) × 10^6/mL after 30 min. The results indicate that big bubbles shrink accompanied by the generation of smaller bubbles. Here, we speculated that the disappearance of microbubbles prompts the formation of NBs.

The IR spectrum was measured to investigate the structural change of water molecules during the shrinking of microbubbles. The fresh NB dispersion was detected by ATR−FTIR measurement every 5 min, and the spectrum of DI water was measured as control. The results are shown in Figure 7b. The ATR−FTIR spectra of all samples have three main features: band around 3400, 1640, and 600 cm^{-1} (shown in the inset in Figure 7b). These peaks are attributed to the stretching vibration and bending vibration of O−H. For SF_6 bubble dispersions, all the spectra showed red shift compared to that of water. Hydrogen-bonded OH originates from two kinds of water: bulk water in liquid and structured water at the interface of bubbles. Hence, the red shift of the peak should come from the SF_6 bubbles.

The broad bands around 3400 cm^{-1} are usually attributed to the stretch modes of the hydrogen-bonded OH of water. The frequency of the OH stretching vibrations is correlated with the strength of the hydrogen-bond interaction: the OH frequency decreases with the increase of the H-bond strength.[34] In addition, the amplification of the OH stretching vibrations of the water bubble from 2700 to 3800 cm^{-1} with the increase of time is shown. The peak position moves toward low wavenumber over time, indicating the formation of more strongly H-bonded water molecules. The strong H bond at the gas−liquid interface is beneficial for decreasing the surface tension and maintaining the NBs stable enough. As discussed above, microbubbles are generated at the beginning. As time goes on, the microbubbles would gradually shrink and eventually form stable NBs in water. The ATR−IR results indicate that more strong hydrogen bonds are formed with the shrinking of microbubbles and generation of NBs.

DISCUSSION

In this study, lots of microbubbles less than 50 μm are first generated by cyclic compression and decompression. As observed through the microscope, the bubbles decrease in size and eventually disappear underwater because of the rapid dissolution of the interior gas. However, DLS and nanosight results show that the stable NBs are maintained in aqueous solutions. Considering these results, it is speculated that the disappearance of microbubbles results in the formation of NBs. After each compression, a certain number of microbubbles are created, which eventually disappear, accompanied by the production of stable NBs. Once the NBs are formed in solution, they do not easily disappear. Therefore, the final concentration of NBs is the cumulative result of cycle compression. The concentration of NBs is proportional to the compression times. The NB concentration can reach about 1.92 × 10^{10} bubbles/mL after compression of 600 times, which is higher than the concentrations (2.94 × 10^8 bubbles/mL by mixing CO_2 with water[10] and 10^9 bubbles/mL by acoustic cavitation[30]) reported in the literature.

The DLS and zeta potential measurements show that the generated NBs are stable and that their life span is longer than 48 h. Other researchers have also demonstrated that NBs can remain in liquid for a long time. Nirmalkar et al. reported that bulk NB suspensions were stable over periods of many months.[30] Oh and Kim. fabricated NBs using CO_2 and showed that the life span of the generated NBs is longer than 24 h.[10] The evolution from the freshly generated microbubble to stable NBs was monitored by a microscope and the IR spectrum. Stronger hydrogen bonds are detected with the decrease of the bubble size. Here, we presume that stronger hydrogen bonds of water are formed at the gas−water interface when the bubble shrinks to nanoscale. A similar interpretation can be inferred from the recent literature. Smolentsev et al. reported the interfacial structure of nanosized water droplets

DOI: 10.1021/acs.langmuir.8b04314
Langmuir 2019, 35, 4238−4245

(200 nm) in a hydrophobic liquid by vibrational sum frequency scattering measurements.[34] The hydrophobic liquid−water interface at the nanoscale reveals significantly stronger hydrogen bonds than that at macroscopic planar interfaces. Strong hydrogen bonds may also form at the gas−liquid interface of NBs. A hard interface composed of strongly hydrogen-bonded water can reduce the diffusivity of gas from the NBs and help to maintain a kinetic balance against the high internal pressure. Moreover, it is found that a strong acidic condition is not suitable to generate a high concentration of monodispersed NBs. The adsorption of OH^- at the bubble interface in alkaline solutions results in a higher zeta potential than that in neutral solutions. Both the arrangement of water molecules in forming hydrogen bonds and the accumulation of OH^- ions at the shrinking gas−water interface may attribute to the high negative surface charge on NBs, which creates repulsive forces to stabilize the NBs.

CONCLUSIONS

In this study, a simple and novel approach to prepare bulk NBs was developed by repeatedly compressing SF_6 gas into water under high pressure and returning to atmosphere pressure. The influence factors of NB generation such as the maximum pressure in the vials, the moving speed of the plunger, and the preadjusting pH in water were investigated. The formation and the stability mechanism of NBs were studied. NBs with an average size of (240 ± 9) nm and PDI of 0.25 are prepared with a maximum pressure of 0.3 MPa, moving speed of 30 mm/s, water pH of 7. The concentration of the NBs generated in water can be controlled by the compression times. The generated NBs have a high negative zeta potential (−40 ± 2 mV) and can be stable for more than 48 h. The freshly prepared microbubbles of about 10−50 μm shrinked and disappeared, accompanied by the generation of stable monodispersed NBs. IR spectroscopy of bubble dispersion showed a red shift compared to that of water. It is speculated that a stronger hydrogen bond is formed at the NB interface. Therefore, it provides a new and general method to prepare gas NBs such as CO_2, O_2, or N_2 to make a promising platform for the basic research and application of NBs.

ASSOCIATED CONTENT

Supporting Information

The Supporting Information is available free of charge on the ACS Publications website at DOI: 10.1021/acs.langmuir.8b04314.

IR spectrum of CO_2 NBs; effect of preadjusting pH in water on NBs; and size distributions of freshly generated microbubbles after preparation (PDF)

Optical microscopic images of the bubble at a time interval of 45 s (AVI)

AUTHOR INFORMATION

Corresponding Authors

*E-mail: yangfang2080@seu.edu.cn (F.Y.).
*E-mail: guning@seu.edu.cn (N.G.).

ORCID

Fang Yang: 0000-0001-6922-6348
Ning Gu: 0000-0003-0047-337X

Notes

The authors declare no competing financial interest.

ACKNOWLEDGMENTS

This investigation was financially funded by the project of National Key Research and Development Program of China (2017YFA0104302), National Natural Science Foundation of China (51832001, 61821002 and 31370019). Further, the funding partially also comes from the Six Talent Peaks Project of Jiangsu Province (2017-SWYY-006) and Zhong Ying Young Scholar of Southeast University. The authors also thank the support from the Collaborative Innovation Center of Suzhou Nano Science and Technology.

REFERENCES

(1) Alheshibri, M.; Qian, J.; Jehannin, M.; Craig, V. S. J. A history of nanobubbles. *Langmuir* **2016**, *32*, 11086−11100.
(2) Temesgen, T.; Bui, T. T.; Han, M.; Kim, T.-i.; Park, H. Micro and nanobubble technologies as a new horizon for water-treatment techniques: A review. *Adv. Colloid Interface Sci.* **2017**, *246*, 40−51.
(3) Agarwal, A.; Ng, W. J.; Liu, Y. Principle and applications of microbubble and nanobubble technology for water treatment. *Chemosphere* **2011**, *84*, 1175−1180.
(4) Ghadimkhani, A.; Zhang, W.; Marhaba, T. Ceramic membrane defouling (cleaning) by air Nano Bubbles. *Chemosphere* **2016**, *146*, 379−384.
(5) Liu, S.; Oshita, S.; Makino, Y.; Wang, Q.; Kawagoe, Y.; Uchida, T. Oxidative capacity of nanobubbles and its effect on seed germination. *ACS Sustainable Chem. Eng.* **2016**, *4*, 67−93.
(6) Tian, J.; Yang, F.; Cui, H.; Zhou, Y.; Ruan, X.; Gu, N. A novel approach to making the gas-filled liposome real: based on the interaction of lipid with free nanobubble within the solution. *ACS Appl. Mater. Interfaces* **2015**, *7*, 26579−26584.
(7) Yang, H.; Cai, W.; Xu, L.; Lv, X.; Qiao, Y.; Li, P.; Wu, H.; Yang, Y.; Zhang, L.; Duan, Y. Nanobubble-affibody: novel ultrasound contrast agents for targeted molecular ultrasound imaging of tumor. *Biomaterials* **2015**, *37*, 279−288.
(8) Li, M.; Liu, Y.; Chen, J.; Liu, T.; Gu, Z.; Zhang, J.; Gu, X.; Teng, G.; Yang, F.; Gu, N. Platelet bio-nanobubbles as microvascular recanalization nanoformulation for acute ischemic stroke lesion theranostics. *Theranostics* **2018**, *8*, 4870−4883.
(9) Craig, V. S. J. Very small bubbles at surfaces-the nanobubble puzzle. *Soft Matter* **2010**, *7*, 40−48.
(10) Oh, S. H.; Kim, J.-M. Generation and stability of bulk nanobubbles. *Langmuir* **2017**, *33*, 3818−3823.
(11) Seddon, J. R. T.; Lohse, D.; Ducker, W. A.; Craig, V. S. J. A deliberation on nanobubbles at surfaces and in bulk. *ChemPhyschem* **2012**, *13*, 2179−2187.
(12) Ishida, N.; Inoue, T.; Miyahara, M.; Higashitani, K. Nano bubbles on a hydrophobic surface in water observed by tapping-mode atomic force microscopy. *Langmuir* **2000**, *16*, 6377−6380.
(13) Lou, S.; Gao, J.; Xiao, X.; Li, X.; Li, G.; Zhang, Y.; Li, M.; Sun, J.; Li, X.; Hu, J. Studies of nanobubbles produced at liquid/solid interfaces. *Mater. Charact.* **2002**, *48*, 211−214.
(14) Ohgaki, K.; Khanh, N. Q.; Joden, Y.; Tsuji, A.; Nakagawa, T. Physicochemical approach to nanobubble solutions. *Chem. Eng. Sci.* **2010**, *65*, 1296−1300.
(15) Uchida, T.; Oshita, S.; Ohmori, M.; Tsuno, T.; Soejima, K.; Shinozaki, S.; Take, Y.; Mitsuda, K. Transmission electron microscopic observations of nanobubbles and their capture of impurities in wastewater. *Nanoscale Res. Lett.* **2011**, *6*, 295.
(16) Karpitschka, S.; Dietrich, E.; Seddon, J. R.; Zandvliet, H. J.; Lohse, D.; Riegler, H. Nonintrusive optical visualization of surface nanobubbles. *Phys. Rev. Lett.* **2012**, *109*, 066102.
(17) Chan, C. U.; Ohl, C.-D. Total-internal-reflection-fluorescence microscopy for the study of nanobubble dynamics. *Phys. Rev. Lett.* **2012**, *109*, 174501.
(18) Liu, Y.; Zhang, X. Nanobubble stability induced by contact line pinning. *J. Chem. Phys.* **2013**, *138*, 2573.

DOI: 10.1021/acs.langmuir.8b04314
Langmuir 2019, 35, 4238−4245

(19) Liu, Y.; Wang, J.; Zhang, X.; Wang, W. Contact line pinning and the relationship between nanobubbles and substrates. *J. Chem. Phys.* **2014**, *140*, 054705.
(20) Weijs, J. H.; Lohse, D. Why surface nanobubbles live for hours. *Phys. Rev. Lett.* **2013**, *110*, 054501.
(21) Liu, Y.; Zhang, X. A unified mechanism for the stability of surface nanobubbles: Contact line pinning and supersaturation. *J. Chem. Phys.* **2014**, *141*, 134702.
(22) German, S. R.; Wu, X.; An, H.; Craig, V. S. J.; Mega, T. L.; Zhang, X. Interfacial nanobubbles are leaky: permeability of the gas/water interface. *ACS Nano* **2014**, *8*, 6193−6201.
(23) Yasui, K.; Tuziuti, T.; Kanematsu, W. Mysteries of bulk nanobubbles (ultrafine bubbles); Stability and radical formation. *Ultrason. Sonochem.* **2018**, *48*, 259−266.
(24) Cho, S.-H.; Kim, J.-Y.; Chun, J.-H.; Kim, J.-D. Ultrasonic formation of nanobubbles and their zeta-potentials in aqueous electrolyte and surfactant solutions. *Colloids Surf., A* **2005**, *269*, 28−34.
(25) Kim, J.-Y.; Song, M.-G.; Kim, J.-D. Zeta potential of nanobubbles generated by ultrasonication in aqueous alkyl polyglycoside solutions. *J. Colloid Interface Sci.* **2000**, *223*, 285−291.
(26) Kikuchi, K.; Ioka, A.; Oku, T.; Tanaka, Y.; Saihara, Y.; Ogumi, Z. Concentration determination of oxygen nanobubbles in electrolyzed water. *J. Colloid Interface Sci.* **2009**, *329*, 306−309.
(27) Chen, Q.; Wiedenroth, H. S.; German, S. R.; White, H. S. Electrochemical nucleation of stable N_2 nanobubbles at Pt nanoelectrodes. *J. Am. Chem. Soc.* **2015**, *137*, 12064−12069.
(28) Chen, Q.; Luo, L.; Faraji, H.; Feldberg, S. W.; White, H. S. Electrochemical measurements of single H_2 nanobubble nucleation and stability at Pt nanoelectrodes. *J. Phys. Chem. Lett.* **2014**, *5*, 3539−3544.
(29) Ushikubo, F. Y.; Furukawa, T.; Nakagawa, R.; Enari, M.; Makino, Y.; Kawagoe, Y.; Shiina, T.; Oshita, S. Evidence of the existence and the stability of nano-bubbles in water. *Colloids Surf., A* **2010**, *361*, 31−37.
(30) Nirmalkar, N.; Pacek, A. W.; Barigou, M. On the existence and stability of bulk nanobubbles. *Langmuir* **2018**, *34*, 10964−10973.
(31) Alheshibri, M.; Craig, V. S. J. Differentiating between Nanoparticles and Nanobubbles by Evaluation of the Compressibility and Density of Nanoparticles. *J. Phys. Chem. C* **2018**, *122*, 21998−22007.
(32) Alheshibri, M.; Craig, V. S. J. Armoured nanobubbles; ultrasound contrast agents under pressure. *J. Colloid Interface Sci.* **2019**, *537*, 123−131.
(33) Takahashi, M. ζ Potential of Microbubbles in Aqueous Solutions: Electrical Properties of the Gas−Water Interface. *J. Phys. Chem. B* **2005**, *109*, 21858.
(34) Smolentsev, N.; Smit, W. J.; Bakker, H. J.; Roke, S. The interfacial structure of water droplets in a hydrophobic liquid. *Nat. Commun.* **2017**, *8*, 15548.

DOI: 10.1021/acs.langmuir.8b04314
Langmuir 2019, 35, 4238−4245